# Sediment erosion in the labyrinths of Francis turbine: A numerical study



# Sediment erosion in the labyrinths of Francis turbine: A numerical study

**Saroj Gautam[1,*], Nirmal Acharya[2], Sailesh Chitrakar[1], Hari Prasad Neopane[1], Igor Iliev[2] and Ole Gunnar Dahlhaug[2]**
[1]*Turbine Testing Lab, Kathmandu University, Dhulikhel, 45210, Nepal*
[2]*Waterpower Laboratory, Department of Energy & Process Engineering, Norwegian University of Science and Technology, NO-7491, Trondheim, Norway*
** Corresponding author (saroj. gautam2019 @hotmail.com)*

**Abstract.** Development of new hydropower projects in Himalayan regions aims for the efficient performance of the turbine with lesser operation and maintenance cost. Over the past two decades, significant efforts have been made to improve the sediment handling capabilities by the turbine components. In the case of Francis turbines, the design of guide vanes and runner blades were focused on the past to improve the sediment resistivity. However, other components of these machines were not studied from the perspective of sediment erosion. The present work aims to study the sediment erosion in the labyrinth sealings of a prototype Francis turbine, having serious erosion problems. Upper labyrinth sealing and bottom labyrinth sealing were modelled by developing a reference case and the erosion wear in these regions were examined numerically. The flow leaving the gap between stationary guide vanes and the runner enters the top and bottom labyrinth seals. While sediment flows along with the clean water these seals get heavily eroded. The results from the numerical investigation show a distinct pattern of erosion locations in the labyrinth sealings that is similar to the field observation.

**Keywords**: Hydropower, Guide Vanes, Sediment Erosion, Labyrinth Sealings

## 1. Introduction

Leakage losses from labyrinth seals in Francis turbines are inevitable. In the case of high head Francis turbine at the design operating condition, the total loss in efficiency due to flow entering and leaving the labyrinths could be nearly about 1.6% [1]. The efficiency drop could be greater at off-design operating condition. Further adding to this loss with clean water condition, the sediment contained flow will affect significantly to the performance of the turbine. Presence of hard minerals in the sediment flowing across the Himalayan regions is found to have serious effects in the turbine's performance [2]. Mineral constituents in the sediment samples of Himalayan rivers are mainly quartz, feldspar, muscovite, biotite, hornblende, magnetite, etc. [3-4]. Out of these constituents, total share of the quartz is highest. The hardness value of the mineral is 7, which is higher than that of the turbine material. Thus, the presence of quartz in the sediment damages the turbine components.

The damage occurring in the turbine component and the flow phenomena is simultaneous in nature [5]. While fluid flows inside different components of the Francis turbine the complex nature of the flow can be observed. This complex nature of flows could be the development of swirls and vortices. The turbulent flow nature inside Francis turbine generates these complex flows. The gap between stationary (Guide vanes) and rotary (Runner vanes), termed as Side Wall Clearance (SWC), is the region where significant leakage occurs. Flow through SWC leads to the upper and bottom labyrinths. Brekke [1], reported that for a typical high head Francis turbine, the loss occurring due to upper SWC and labyrinth to be 0.8% and bottom SWC and labyrinth to be 0.8%. These losses are due to the leakage loss

and disk friction loss, which are caused due to SWC and flow at the labyrinths [6]. It was reported that these losses have significant effect on the performance of the turbine [7-8].

This study presents a numerical study on the flow phenomenon and the resulting sediment erosion effects in the labyrinths of a prototype Francis turbine with specific speed Ns=85.4. The first part of this papers presents the numerical model and mesh followed the erosion effects at upper and bottom labyrinth region with the discussion in the flow phenomenon.

## 2. Development of the reference case

A prototype Francis turbine of Bhilangana- III Hydropower Project (B-III HPP) has been selected for this study. The reports on erosion damage in this power plant is presented in a case study by [3]. Moreover, the flow phenomenon through the clearance gap region and the resulting pressure fluctuations in the runner was examined by [10]. The nature of flow field and resulting sediment erosion damage was examined by [11], considering the overall turbine components from Guide vane up to Draft tube. This study is a continuation the works carried out before on the same turbine. In this study, more emphasize has been given on the labyrinth regions only considering both upper and bottom labyrinth.

### *2.1 Numerical model and mesh*

A three-dimensional geometry of the prototype Francis turbine was prepared using ANSYS ICEM CFD. The geometry included Scroll Casing (SC), Stay Vanes (SVs), Guide Vanes (GVs), Upper Labyrinth (UL), Bottom Labyrinth (BL), Runner and a Draft Tube (DT). ICEM CFD was used to prepare the hexahedral mesh of the UL, BL and DT. For GV and Runner, ANSYS TURBOGRID was used to generate structured hexahedral mesh. For this study, the numerical investigation was done considering only GVs, UL, BL, Runner and DT. For the boundary conditions in the numerical model field measurements data were used. Standard mass flow inlet and pressure outlet boundary condition was used for the numerical study [12]. Mass flow inlet of 4330 kg/s at BEP was prescribed with cylindrical co-ordinate system at the inlet of GV. The outlet of the DT was prescribed as an opening type pressure boundary condition. Figure 1 shows the locations of the boundaries and grid generated for this numerical study.

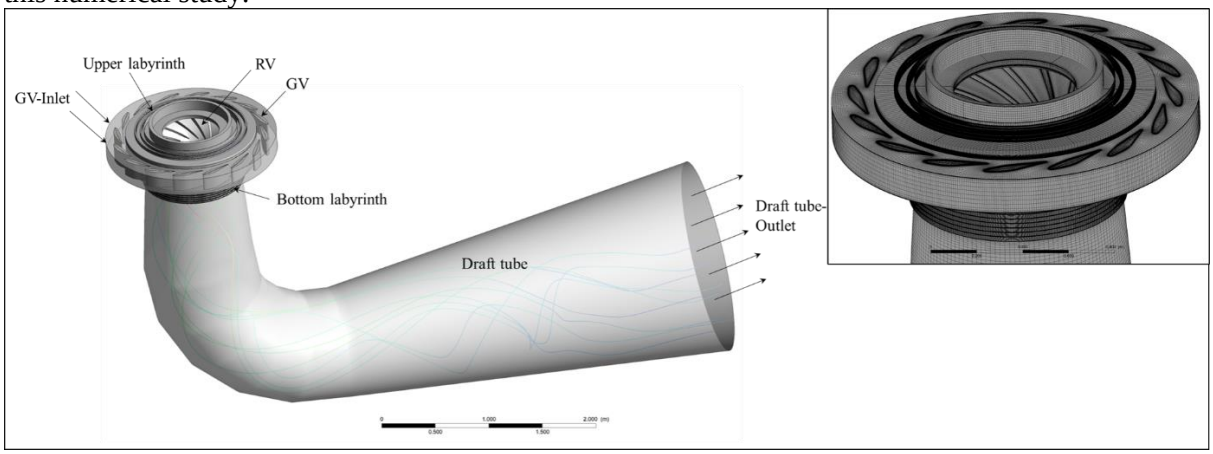


**Figure 1.** Computational domain with the hexahedral mesh in the prototype Francis turbine

The simulations were performed using transient flow condition considering 5 revolutions of the runner at rotational speed 750 RPM. Unsteady Reynolds-Averaged Navier-Stokes (URANS) equations was used to model the flow field and solved using element-based finite volume method which is given as;

$$\frac{\partial \overline{u}_i}{\partial \overline{x}_i} = 0 \tag{1}$$

$$\frac{\partial \overline{u}_i}{\partial t} + \overline{u}_j \frac{\partial \overline{u}_i}{\partial x_j} = -\frac{1}{\rho}\frac{\partial \overline{p}}{\partial x_i} + \upsilon \frac{\partial^2 \overline{u}_i}{\partial x_j^2} - \frac{\partial (\overline{u}'_i \overline{u}'_j)}{\partial x_j} \tag{2}$$

where, $\overline{u_i}$ =time-averaged velocity components

p=pressure component

υ=kinematic viscosity

$\overline{u_i}'$=fluctuating velocity component

For erosion modelling, Tabakoff and Grantt erosion model was used based on the effectiveness of the numerical model from previous literatures [3]. The properties of sediment used in the numerical model are given in Table 1.

**Table 1** Sediment properties used for this study

| **Parameters** | **Unit** | **Value** |
|---|---|---|
| Density | kg/m$^3$ | 2650 |
| Number | [-] | 5000 |
| Shape factor | [-] | 0.7 |
| Size | µm | 150 |

*2.2 Numerical model and mesh*

In this study three different grids: Fine (G1), Medium (G2) and Coarse (G3) were used for grid independency test. Starting from the coarsest mesh G3, the subsequent mesh was updated by increasing the number of elements globally by 1.5 times. In doing so, the quality of the mesh was unaltered. Simulations were performed with these three mesh schemes and the extrapolation values and uncertainty in the grid convergence study were estimated using Grid Convergence Index (GCI) technique [13-14]. For this the approximate and extrapolated relative errors were estimated as;

$$e_a^{21} = \left| \frac{G_1 - G_2}{G_1} \right| \tag{3}$$

$$e_{ext}^{21} = \left| \frac{G_{ext}^{12} - G_1}{G_{ext}^{12}} \right| \tag{4}$$

Finally, GCI was estimated as;

$$GCI_{fine}^{21} = \frac{1.25 e_a^{21}}{r_{21}^p - 1} \tag{5}$$

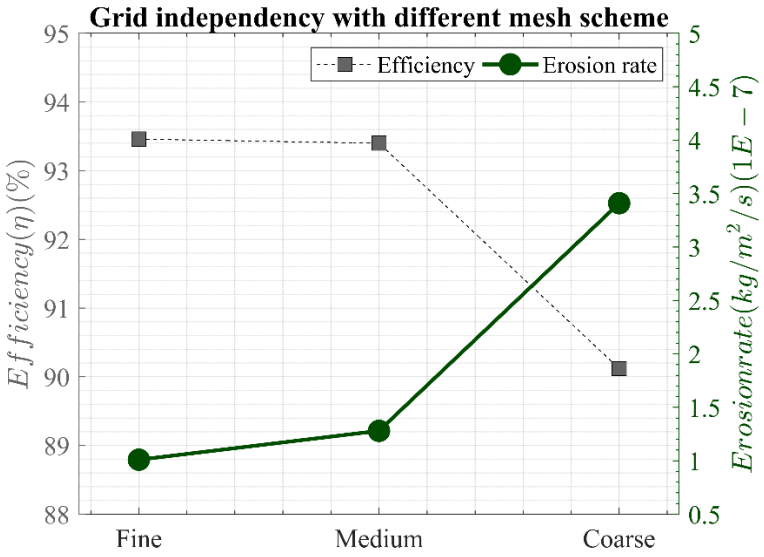


**Figure 2.** Efficiency and erosion variation at different mesh scheme

Figure 2 shows the efficiency and the erosion rate variation with coarse, medium, and fine mesh. As shown in the figure, the efficiency predicted using coarsest mesh is lesser than that of medium and fine mesh. Similarly, in terms of sediment erosion the erosion predicted with the coarsest mesh is higher.

For both variables, medium and fine mesh have nearly same values. Corresponding GCI values from medium mesh to fine mesh using equations (3-5) were 0.0011% and 2.98% respectively.

The details of the grid independency test and the validation of the numerical model with experiment for this numerical model is presented in studies [10-11].

## 3. Results and discussion

### *3.1 Sediment erosion in upper labyrinth region*

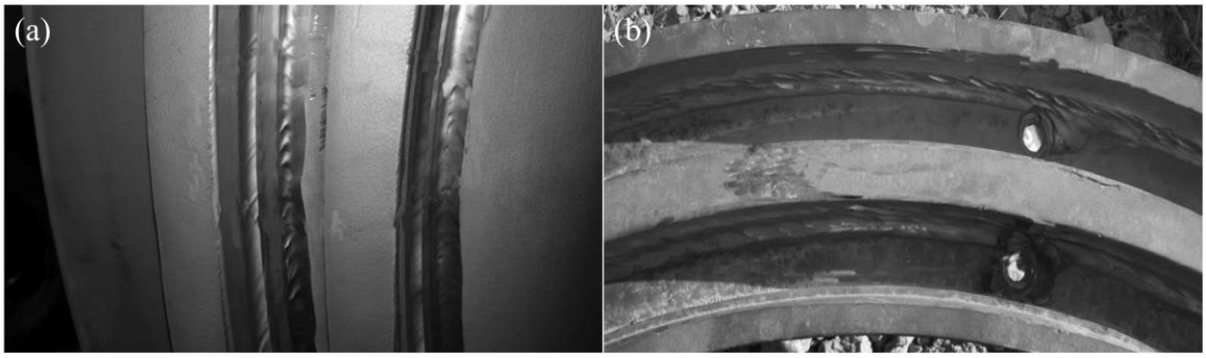


**Figure 3.** Sediment erosion at the upper labyrinth, (a) Towards rotating end and (b) Towards stationary end

Figure 3 shows the eroded region towards the rotating and stationary part of upper labyrinth of the prototype turbine considered for this study. For both top labyrinth on runner and top labyrinth ring, erosion occurs towards the corner region. The erosion towards this region is mainly due to the re-circulating flow due to the sudden expansion. This re-circulating flow is deliberately created while designing the labyrinth seals such that pressure energy is dissipated into head and create the needed pressure difference to seal the zone. This pressure difference is achieved with the faction of the volumetric discharge through the turbine that comes from the hydrodynamic design of labyrinth seals. The interesting phenomena that can be observed in this case is that the flow re-circulation in this region and the corresponding sediment erosion is simultaneous. Either cannot be neglected for the turbine to be designed for sediment laden water. Thus, for labyrinth that is deliberately designed to have high flow recirculation with minimum leakage, there occurs the highest erosion wear that in turn induces the volumetric loss.

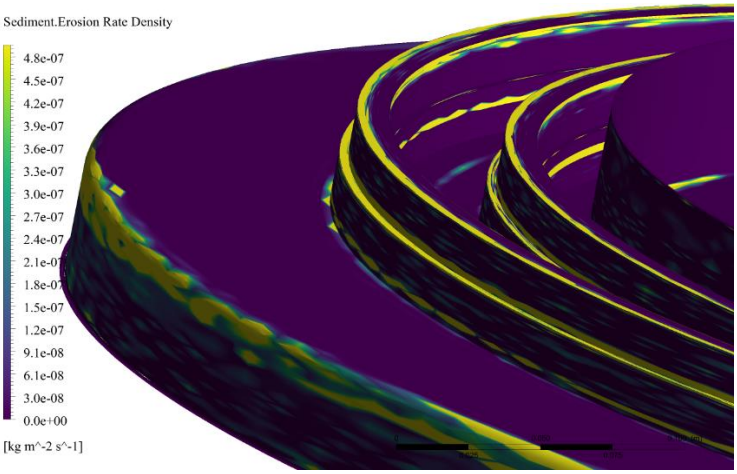


**Figure 4.** Erosion wear towards runner hub and upper labyrinth predicted from the numerical study

Figure 4 shows the erosion predicted from the numerical study in the hub region and the upper labyrinth region of the runner. It can be noticed from the field report of the erosion in Figure 3 that the numerical model was suitable enough the predict the erosion at those regions. However, CFD model over predicted the erosion wear mainly towards the upper labyrinth compared to the field report. This discrepancy might be due to variables selected for the erosion quantification in the Tabakoff and Grantt erosion model.

*3.2 Flow inside upper labyrinth and resulting pressure fluctuations*

In order the examine the erosion effects in the labyrinth region, it is necessary to examine the corresponding flow field inside. In this case the relative vorticity measurement is used to analyse the vortex flow region inside the labyrinth region. The vorticity transport equation as given as;

$$\frac{D\Omega_r}{Dt} = (\Omega_r \bullet \nabla)\vec{W} - \Omega_r(\nabla \bullet \vec{W}) - 2\nabla \times (\omega \times \vec{W}) + \frac{\nabla \rho_m \times \nabla \rho}{\rho_m^2} + \upsilon \nabla^2 \Omega_r \quad (6)$$

Here, $\Omega_r$, $\vec{W}$ and $\upsilon$ refers to relative vorticity, relative velocity and the kinematic viscosity respectively.

The term in the Left-hand side refers to the rate of the change in vorticity. At the Right-hand side, first term denotes a relative vortex stretching, second term is the relative vortex dilation, third term refers to the effects due to Coriolis force that influences the relative vorticity, fourth term originates from baroclinic torque and reaches zero in case of barotropic fluids and the final term is the viscous diffusion which results in the rate of change in the relative vorticity.

Figure 5 shows the distribution of vorticity magnitude inside the upper labyrinth region. The flow pattern inside the stepped region 1 and 2 demonstrates the highest recirculation with resulting the highest-pressure oscillation. This indicates that the flow inside the upper labyrinth region is recirculating that is an obvious flow pattern for the labyrinth design as discussed above. This flow pattern was examined in detail considering the pressure oscillations at certain points inside the stepped upper labyrinth. A total of six points were selected for pressure investigation that were located at the centroid of each step of tooth of the labyrinth. Thus, for two teeth with three steps in each labyrinth teeth, there exist a total of six regions.

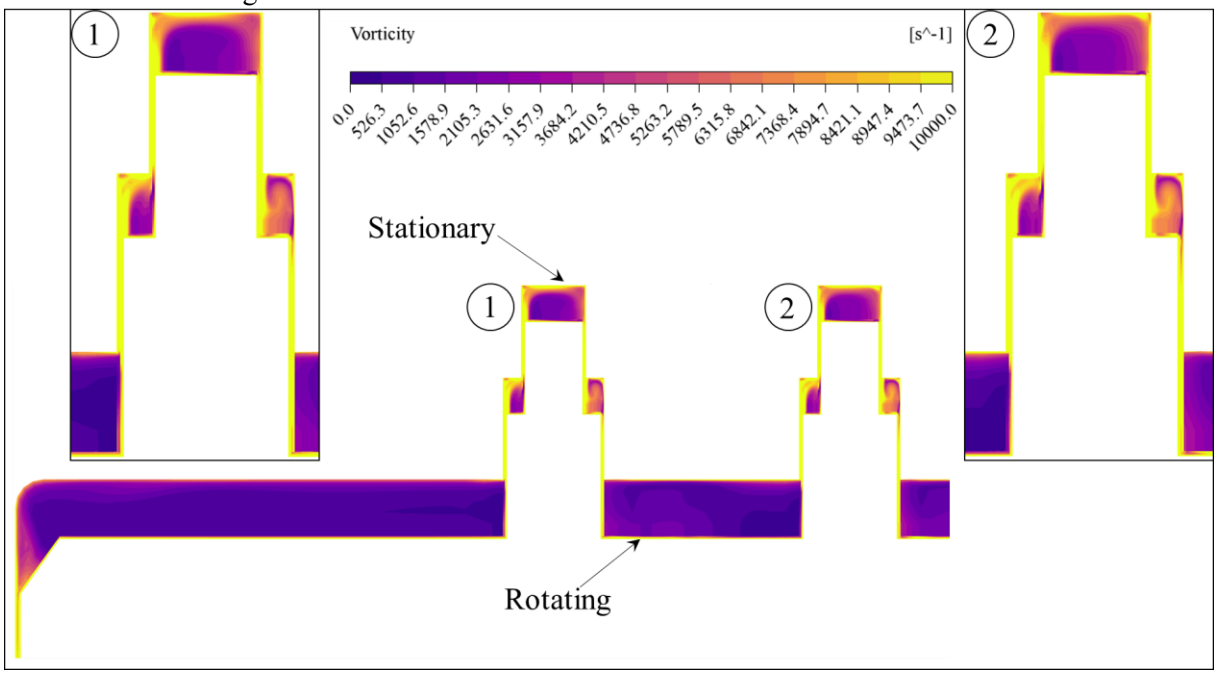


**Figure 5.** Vorticity magnitude inside the upper labyrinth region

Figure 6 presents the graph of the pressure oscillations at all these points during the runner rotation. Here the pressure value is normalized using the equation;

$$p = \frac{p}{(\rho g H)_{BEP}} \ [-] \quad (7)$$

where $p$, p, $\rho$, g and H refers to the normalized pressure in Pa, acquired pressure in Pa, water density in kg $m^{-3}$, acceleration due to gravity (9.81 m $s^{-2}$) and head in m respectively.

As stated above while flow passes beneath the upper labyrinth, the corresponding flow recirculation occurs contributing to the reduction in the pressure magnitude. Since at the upper labyrinth

the flow velocity undergoes successive radial and axial change in the velocity magnitude, the decrease in the pressure is obvious. Similarly for all the cases, there is corresponding highest pressure amplitudes. It can be noticed from the pressure fluctuations in region 1 presented as the first half of upper labyrinth at all three points there is resulting 16 pressure oscillations corresponding to number of guide vanes. Across region 2 huge pressure drop occurs and also there is no significant pressure oscillations corresponding to GV number. Overall, the gradual change in the pressure resulting in the flow recirculation and vortex development near the corners of the labyrinth region gives rise to erosion wear due to sediment contained flow.

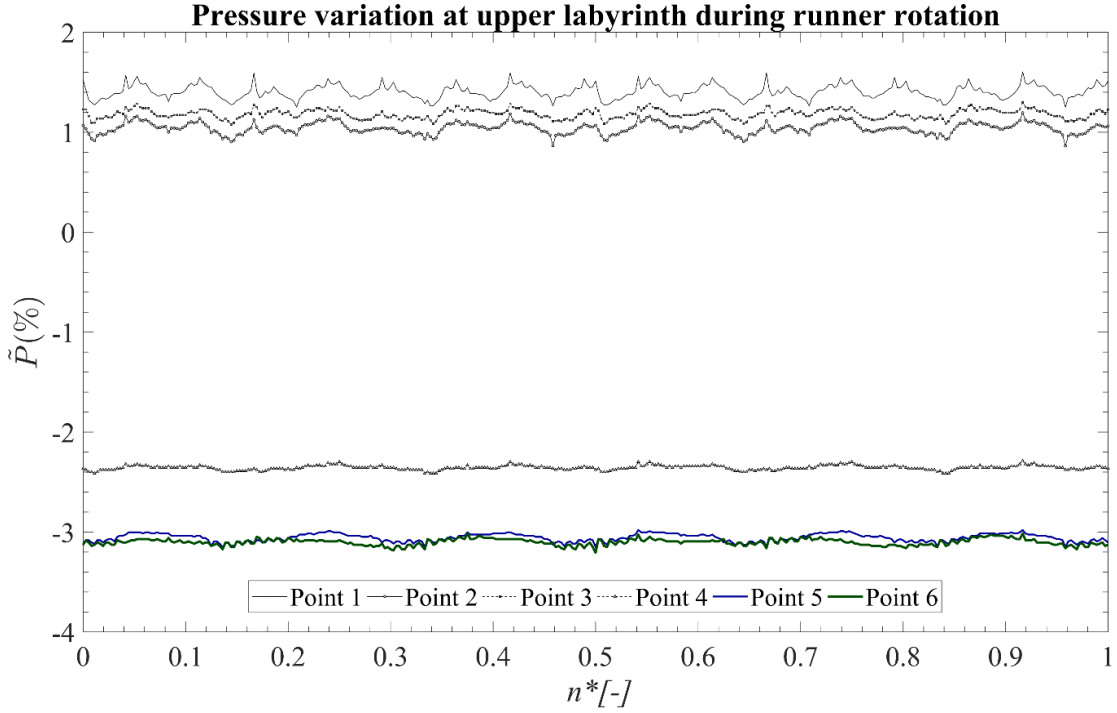


**Figure 6.** Graph of the pressure field inside upper labyrinth region. (Y-axis refers to non-dimensional pressure measurement given by equation 7 and X-axis refers to non-dimensional runner rotation where 0 belongs to the start of the runner rotation and 1 refers to one complete rotation of the runner)

*3.3 Sediment erosion in bottom labyrinth region*

When fluid leaves GV, a part of its flow escapes through bottom side-wall clearance and reaches bottom labyrinth. With the sediment contained flow the erosion traces can be observed mostly towards the corner of the steps. Bottom labyrinth in this study is of double cavity stepped tooth type with seven cavities. The distinct regions of erosion can be observed at both rotating and stationary ends of bottom labyrinth as shown in Figure 7. As discussed earlier, these regions of erosion are mainly due to flow recirculation while flowing from upper end to lower end. In this study, the flow escaping from lower end of the bottom labyrinth mixes with the flow at the DT.

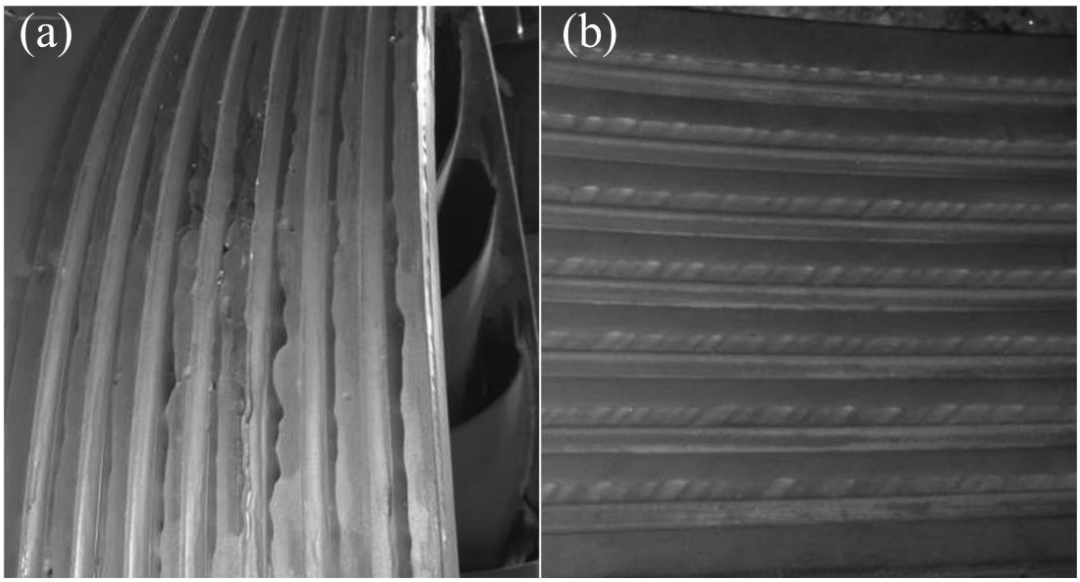


**Figure 7.** Sediment erosion at the bottom labyrinth, (a) Towards rotating end and (b) Towards stationary end

In Figure 8, the erosion wear predicted from numerical study at the bottom labyrinth region is shown. Erosion in this case is mainly seen in the labyrinth cavities 2,3, 5 and 6. However, from the field measurement as shown in Figure 6, there is the uniform erosion wear in all regions. For same operational time it can be noticed that the stationary end of the bottom labyrinth has highest effect of erosion compared to the rotating end. Gautam [11], suggested that this variation is due to difference in the centrifugal force acting on the sediment particle and use of different material for rotating and stationary part.

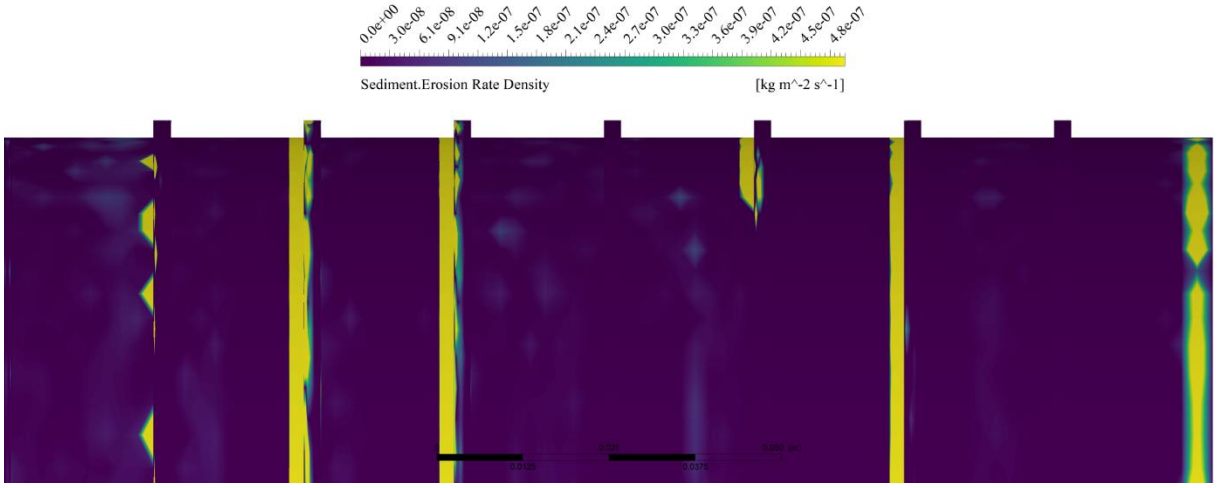


**Figure 8.** Erosion wear towards bottom labyrinth predicted from the numerical study

*3.4 Flow inside bottom labyrinth and resulting pressure fluctuations*

Figure 8 shows the measure of vorticity magnitude inside the plane of bottom labyrinth. Vortex region here is mainly accumulated towards the rotating section. However, towards both the stationary and rotating corners, the accumulation of the sediment particle can be observed that causes erosion at those regions. In figure 9, it can be seen that the vorticity distribution is similar for the cavities numbered 1,3,5 and 7 regardless of the axial geometric position. Thus, it can be inferred that the axial fluid flow does not have significant affect in the flow recirculation inside those cavities. Therefore, at all the axial geometrical positions the erosion wear is similar as seen in Figure 7. In this case the rotational direction of the vortical regions is anti-clockwise which is due to the flow separation that is caused by the change in area and the effect of rotating wall of labyrinth. In the rotating region the direction of the flow is

opposite to the stationary wall. The sudden expansion and contraction of the area of the flow causes the corner vortices.

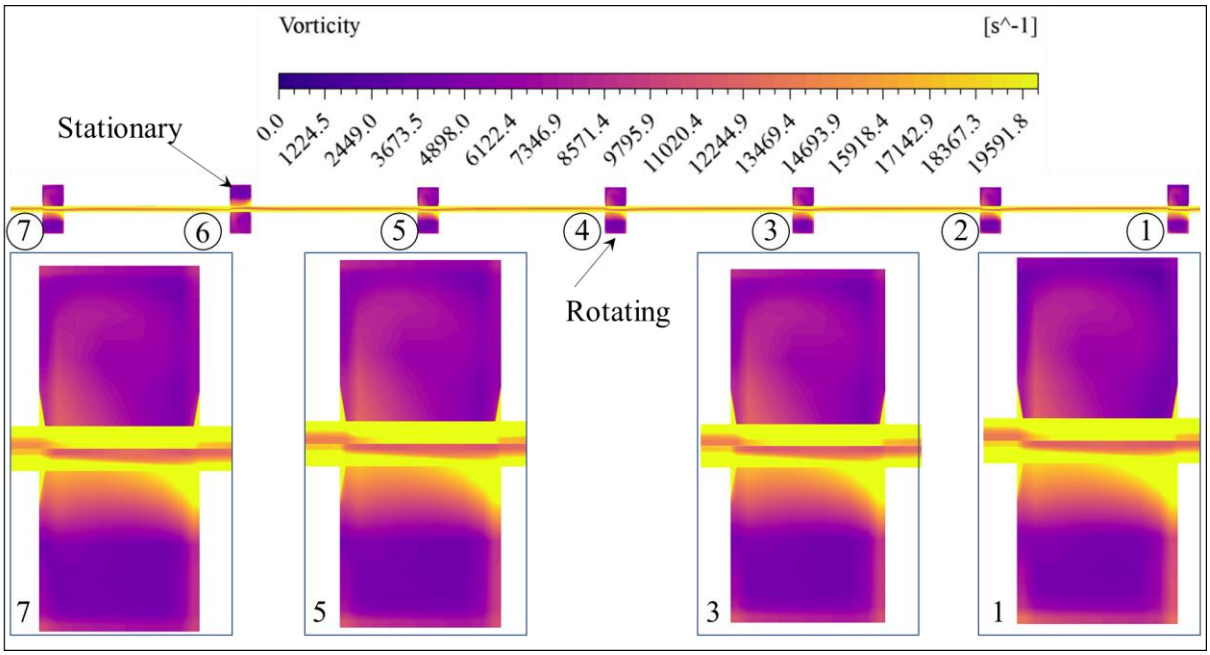


**Figure 9.** Vorticity magnitude inside the bottom labyrinth region

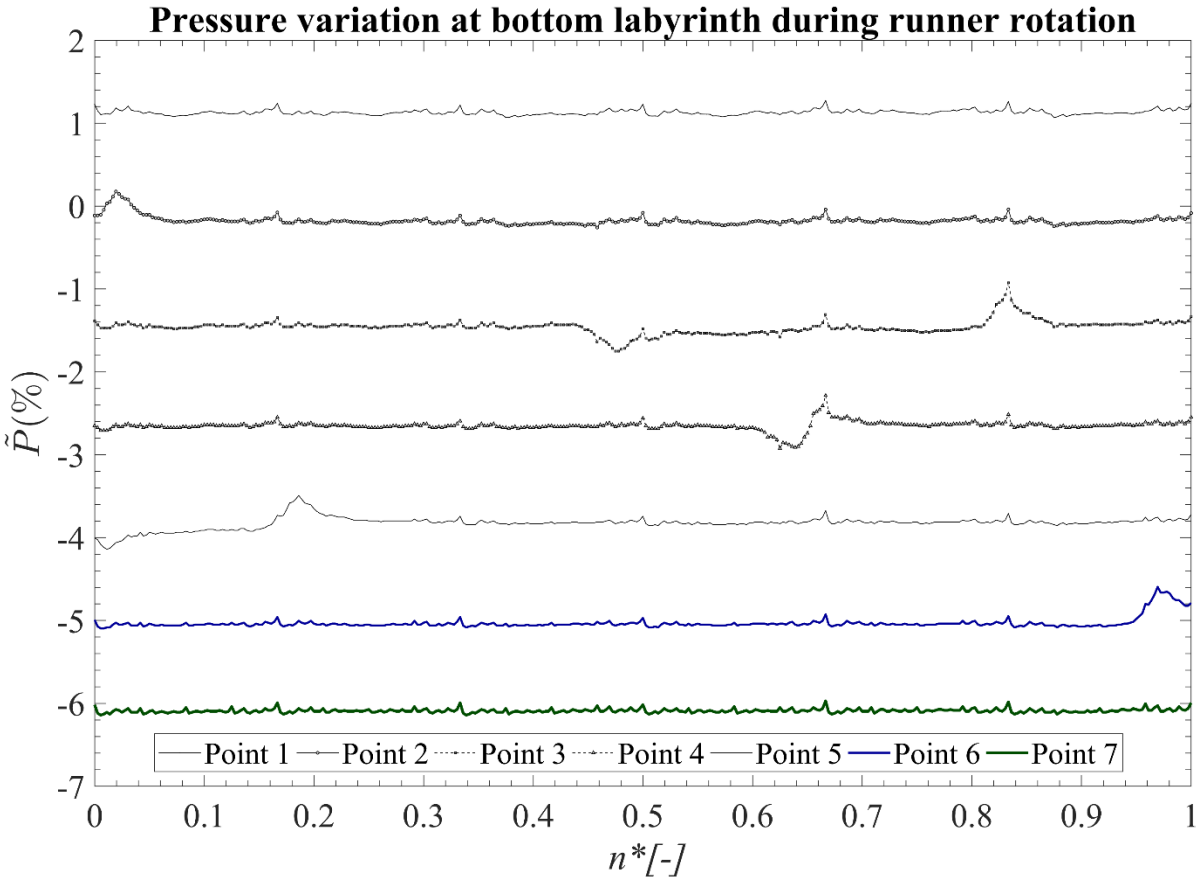


**Figure 10.** Graph of the pressure field inside bottom labyrinth region. (Y-axis refers to non-dimensional pressure measurement given by equation 7 and X-axis refers to non-dimensional runner rotation where 0 belongs to the start of the runner rotation and 1 refers to one complete rotation of the runner)

In Figure 10 the graph of pressure oscillation inside bottom labyrinth is shown. Here the pressure is normalized using equation 7. The pressure measurement was carried out at the centroid of each rotating cavity numbered 1 up to 7. Thus, 7 different bands of pressure can be observed in the graph. It can be noticed the while moving downwards i.e., from Point 1 to Point 7, the magnitude of pressure reduces that signifies the axial flow from the inlet of bottom labyrinth to inlet of draft tube. At all the points of pressure fluctuations are mainly due to the blade passing frequency. There also exists other high-frequency and small-amplitude random fluctuations which are due to turbulent eddies [15]. This existence of turbulence eddies can be confirmed from the vortex plot presented in Figure 9.

## 4. Conclusion

Overall, this study presented a numerical case study of a prototype Francis turbine at design operation condition. The simulations were performed using SST turbulence model. The investigation was carried out considering both steady and unsteady state cases. Following are the pertinent findings from this study:

- Erosion model used for this study was suitable to predict the erosion affected region in the labyrinth similar to the field observation.
- The expansion and contraction of labyrinth geometry gives rise to flow recirculation and corner vortices. This causes the resulting pressure oscillations.
- This flow recirculation enhances the erosion effects towards the corners of top and bottom labyrinths.
- The impact of pressure fluctuations affects the performance of the seals. These oscillations have severe damage in the seal region due to sediment contained flow.

## 5. Acknowledgments

This work is supported by **FranSed Project** (2018-2022) that are currently running with the collaboration of Norwegian University of Science and Technology and Kathmandu University.

## 6. References

[1]. Brekke H, Wu Y L and Cai B Y 2003 *Design of Hydraulic Machinery Working in Sand Laden Water* pp 155–233.
[2]. Thapa B 2004 *Sediment Erosion in Hydro Turbines* (Norwegian University of Science and Technology)
[3]. Gautam S, Neopane H P, Acharya N, Chitrakar S, Thapa B S and Zhu B 2020 Sediment erosion in low specific speed francis turbines: A case study on effects and causes *Wear* 442–443 203152
[4]. Neopane H P, Dahlhaug O G and Cervantes M J 2012 The effect of sediment characteristics for predicting erosion on Francis turbines blades *Int. J. Hydropower Dams* **19** 79–83
[5]. Chitrakar S, Neopane H P and Dahlhaug O G 2016 Study of the simultaneous effects of secondary flow and sediment erosion in Francis turbines *Renew. Energy* **97** 881–91
[6]. Zhao W 2012 *Investigation of seal technology for Francis turbine* (Norwegian University of Science and Technology).
[7]. Schiffer J, Benigni H, Jaberg H and Schneidhofer T 2015 Numerical simulation of the flow in a Francis turbine including the runner seals on crown and band side *Hydro - Int. Conf. Exhib. - Bordeaux, Fr.* 3–10
[8]. Schiffer J, Benigni H and Jaberg H 2017 Analysis of the leakage behavior of Francis turbines and its impact on the hydraulic efficiency - A validation of an analytical model based on computational fluid dynamics results *J. Fluids Eng. Trans. ASME* **139**
[9]. Mack R, Drtina P and Lang E 1999 Numerical prediction of erosion on guide vanes and in labyrinth seals in hydraulic turbines *Wear* **233**–**235** 685–91
[10]. Acharya N, Gautam S, Chitrakar S, Trivedi C and Dahlhaug O G 2021 Leakage Vortex

Progression through a Guide Vane's Clearance Gap and the Resulting Pressure Fluctuation in a Francis Turbine *Energies* **14** 4244

[11]. Gautam S, Acharya N, Chitrakar S, Neopane H P, Iliev I and Dahlhaug O 2021 Correlating Sediment Erosion in Rotary-Stationary Gaps of Francis Turbines with Complex Flow Patterns *SSRN Electron. J.*

[12]. Trivedi C, Cervantes M J, Gandhi B K and Dahlhaug O G 2013 Experimental and numerical studies for a high head francis turbine at several operating points *J. Fluids Eng. Trans. ASME* **135** 1–17

[13]. Celik I B, Ghia U, Roache P J, Freitas C J, Coleman H and Raad P E 2008 Procedure for estimation and reporting of uncertainty due to discretization in CFD applications *J. Fluids Eng. Trans. ASME* **130** 0780011–4

[14]. Bergström J and Gebart R 1999 Estimation of numerical accuracy for the flow field in a draft tube *Int. J. Numer. Methods Heat Fluid Flow* **9** 472–86

[15]. Trivedi C 2018 Compressible large eddy simulation of a Francis turbine during speed-no-load: Rotor stator interaction and inception of a vortical flow *J. Eng. Gas Turbines Power* **140**